Published in IET Control Theory and Applications
Received on 26th August 2009
Revised on 25th December 2009
doi: 10.1049/iet-cta.2009.0437

ISSN 1751-8644

2-Sliding active and reactive power control of a wind energy conversion system

F. Valenciaga C.A. Evangelista

LEICI, Faculty of Engineering, UNLP – CONICET, C.C.91, C.P. 1900 La Plata, Argentina
E-mail: fval@ing.unlp.edu.ar

Abstract: This study presents the control of a variable-speed wind energy conversion system based on a brushless doubly fed reluctance machine. The control objectives are the tracking of the maximum power conversion point and the regulation of the reactive power injected by the generation system into the grid. The control design is approached using multi-input second-order sliding techniques which are specially appropriate to deal with non-linear system models in the presence of disturbances and model inaccuracies. The controller synthesised through this theoretical framework presents very good robustness features, a finite reaching time and a chattering-free behaviour. The performance of the closed-loop system is assessed through representative computer simulations.

1 Introduction

During the last few decades, wind energy conversion has been the renewable power generation source that has experienced the fastest growth. It is expected that this tendency remains for a long time [1]. Traditionally, the main control objective on large wind turbines has been to reduce the cost-effective utilisation of this kind of energy aiming at quality and reliability in the electricity delivery [2, 3]. In this context, among the different existing wind conversion system structures, variable-speed (VS) topologies are continuously increasing their market share because they can maintain the optimal power generation on variable wind speed regimes [4].

One of the most popular topologies used to implement VS wind energy conversion systems (WECS) comprises a doubly fed induction generator (DFIG) directly connected to the local utility grid by stator and a back-to-back four-quadrant ac–dc–ac power converter used to link the rotor windings and the grid. This configuration, usually called slip power recovery topology, is efficient and flexible in the energy conversion process and presents the advantage of only needing a fractionally rated converter. Compared to WECS using synchronous generators, the wind conversion technology based on DFIG has several advantages such as four-quadrant active and reactive power capabilities, lower converter costs and lower power losses. However, in spite of its popularity in uses with reduced VS ranges, the DFIG presents some important drawbacks originated in the presence of slip rings, brushes and a wounded rotor [5, 6].

In the last few years, the brushless doubly fed reluctance machine (BDFRM) emerged in the specialised literature as an attractive option to replace DFIGs in grid-connected variable-speed constant frequency (VSCF) power-generation systems [7, 8]. On the basis of cost and robustness criteria, its use results specially appropriate in large power applications with restricted VS capability such as pumps and wind turbines [9–11]. Within these kinds of applications, the BDFRM allows one to retain the main advantages of using wound rotor induction machines, increasing the system reliability and reducing the maintenance expenses because of its brushless and cageless rotor structure [5, 12].

This work develops a decoupled active and reactive power controller for a fixed pitch VS-WECS based on a BDFRM, connected in the slip power recovery topology shown in Fig. 1. Constructively, the BDFRM presents two standard sinusoidally distributed stator windings of different numbers of poles and a reluctance rotor that provides the magnetic coupling between them, presenting half the total numbers of stator poles [9]. The control action is applied via the bidirectional PWM static converter placed at the terminals of the secondary windings. This last device allows

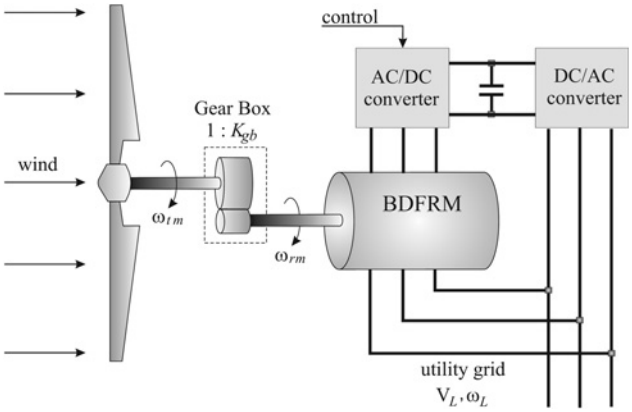

Figure 1 *VSCF-WECS in a slip power recovery topology*

driving the magnitude and angular frequency of the secondary spatial voltage vector, indirectly controlling the total active power and the primary reactive power produced by the generator. The complexity of the control design task lies on the highly non-linear nature of the dynamic model of the system, on its multi-input multi-output (MIMO) structure, and on the existence of model uncertainties and external disturbances. On the other hand, it is important to note that the control technique employed must synthesise a continuous control action that can be adequately implemented through the PWM converter. In this context, the control design is faced using second-order sliding mode (SOSM) techniques. This theoretical framework is especially appropriate for coping with the described control difficulties [13–15]. Besides, the resultant controller presents some additional and attractive features such as finite time reaching phase, a chattering free sliding mode behaviour [16] and a reduced computational cost.

The article is organised as follows: Section 2 introduces the general control strategy; Section 3 is devoted to present the dynamic model of the BDFRM-WECS; Section 4 presents a brief introduction to multi-input SOSM techniques, introduces the control objectives in terms of sliding variables and deals with the controller design; in Section 5 the performance of the proposed closed-loop system analysed through representative simulations and compared with the results of using a traditional PI design and finally in Section 6 conclusions are presented.

2 Control strategy

Traditionally, the primary control objective for large WECS has been to reduce the cost per kilowatt hour. This means to maximise the power conversion only limited by the rated power of the generator [2]. On the other hand, modern WECS are expected to exhibit other control features like the control of the reactive power absorbed from or injected into the grid [17]. In this sense, this work deals with the design of a MIMO controller that allows one to simultaneously fulfil the aforementioned objectives in a decoupled way. With this purpose in mind, this section is devoted to obtain adequate active and reactive power references.

The power captured by a wind turbine of blade length r facing an airflow of speed v and density ρ can be expressed by [18]

$$P_t(\lambda) = \frac{1}{2}\pi\rho r^2 C_p(\lambda) v^3 \tag{1}$$

where $C_p(\lambda)$ is a non-linear function of the tip speed ratio, λ, defined as $\lambda = r\omega_{tm}/v$ where ω_{tm} is the rotational speed of the shaft on the turbine side. This function, commonly referred to as 'turbine power coefficient', characterises the mechanical conversion efficiency of a turbine. A typical profile of this function for a fixed pitch horizontal three-blade turbine is depicted in Fig. 2.

It can be observed that this function presents a unique maximum at $\lambda = \lambda_{opt}$ where the turbine extracts the maximum energy from the wind. Therefore conversion efficiency maximisation is achieved by tracking the turbine optimal tip speed ratio λ_{opt}, which implies to adequately drive the rotational speed in accordance with wind speed variations.

A suitable approach to avoid the utilisation of wind speed measurements in the control law is to synthesise a torque reference function corresponding to the optimal generation

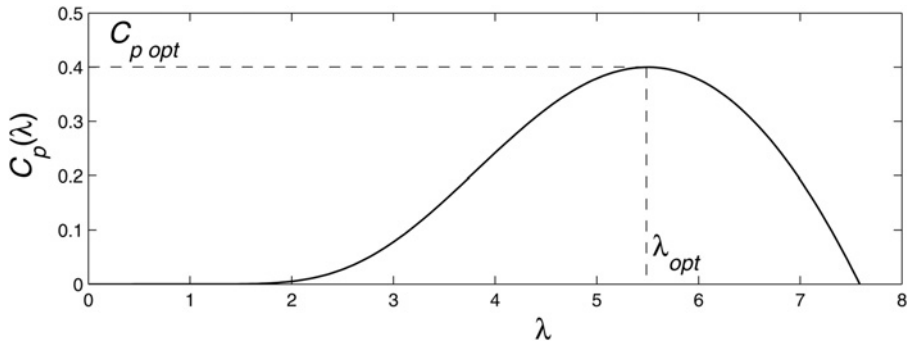

Figure 2 *Typical three-blade turbine conversion efficiency function*

doi: 10.1049/iet-cta.2009.0437

locus in the torque–shaft speed plane [19]. From (1), it is straightforward to obtain the expression of the turbine torque

$$T_t(\lambda) = \frac{P_t}{\omega_{tm}} = \frac{1}{2}\frac{\pi\rho r^2 C_p(\lambda)}{\omega_{tm}} v^3 = \frac{1}{2}\pi\rho r^3 \frac{C_p(\lambda)}{\lambda} v^2 \quad (2)$$

Then, evaluating this expression on the optimal generation locus ($\lambda = \lambda_{opt}$ and $v = r\omega_{tm}/\lambda_{opt}$), the mentioned torque reference function can be written as

$$T_{tref}(\omega_{tm}) = K_{opt}\omega_{tm}^2 \quad (3)$$

with $K_{opt} = \pi\rho r^5 C_p(\lambda_{opt})/2\lambda_{opt}^3$. To track this reference is equivalent to track a filtered version of the optimal operation point, where variations produced by wind gusts and other high-frequency components of the equivalent wind are neglected.

It is important to note that this reference can be followed up to the point where the generator develops its rated power. Beyond that point, the active power generation must be bounded in order to avoid damages to the system. This operation strategy is sketched in Fig. 3 in terms of active power and the corresponding reference torque for different wind speeds.

Unlike the active power case, the reactive power injected by the primary winding into the grid does not present a close and direct correlation with the actual operational point of the wind turbine. Thus, its reference value ($Q_{1ref}(t)$) can be temporally specified according to the directives of a more general control level that regulates the whole grid operation [2]. However, it is important to note that although this reference value can be fixed by this higher control level, its value must instantaneously comply with the limit imposed by the minimum power factor allowed for the primary winding functioning.

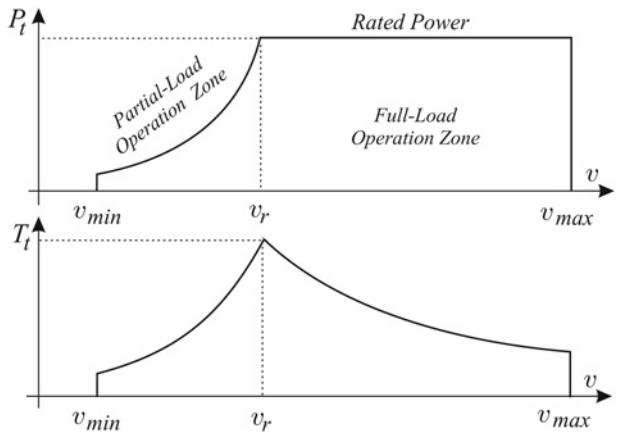

Figure 3 *Active power generation: operation strategy*

3 Dynamic model of the WECS-BDFRM

The BDFRM-WECS in the slip power recovery topology depicted in Fig. 4 has the p_1-pole primary winding of the generator directly linked to the utility grid. Therefore the line imposes its voltage and electrical frequency on it ($v_1 = V_L$; $\omega_1 = \omega_L$). The remaining winding, usually called secondary or control winding, presents p_2 poles and is connected to the grid via a bidirectional PWM converter. This last device drives the secondary voltage (v_2) and its angular frequency (ω_2) indirectly controlling the operational point of the whole system.

The complete dynamic model of this system is composed of the electrical dynamics of the brushless machine and the mechanical dynamics of the rotating parts. Viewed from two quadrature dq reference frames rotating, respectively, at angular speeds ω_1 and ω_2, the former can be expressed by [8]

$$\dot{\lambda}_{1d} = -R_1 i_{1d} + \omega_1 \lambda_{1q} + v_{1d} \quad (4)$$

$$\dot{\lambda}_{1q} = -R_1 i_{1q} - \omega_1 \lambda_{1d} + v_{1q} \quad (5)$$

$$\dot{\lambda}_{2d} = -R_2 i_{2d} + (\omega_r - \omega_1)\lambda_{2q} + v_{2d} \quad (6)$$

$$\dot{\lambda}_{2q} = -R_2 i_{2q} - (\omega_r - \omega_1)\lambda_{2d} + v_{2q} \quad (7)$$

$$\lambda_{1d} = L_1 i_{1d} + L_{12} i_{2d} \quad (8)$$

$$\lambda_{1q} = L_1 i_{1q} - L_{12} i_{2q} \quad (9)$$

$$\lambda_{2d} = L_2 i_{2d} + L_{12} i_{1d} \quad (10)$$

$$\lambda_{2q} = L_2 i_{2q} - L_{12} i_{1q} \quad (11)$$

where the variables v_{1d}, v_{1q}, v_{2d} and v_{2q} represent the quadrature components of the primary and secondary winding voltages; i_{1d}, i_{1q}, i_{2d} and i_{2q} correspond to the current components and λ_{1d}, λ_{1q}, λ_{2d} and λ_{2q} are the concatenated flux components. On the other hand, the parameters R_1 and R_2 represent the stator winding resistances, L_1 and L_2 their self-inductances, and L_{12} the mutual inductance between windings.

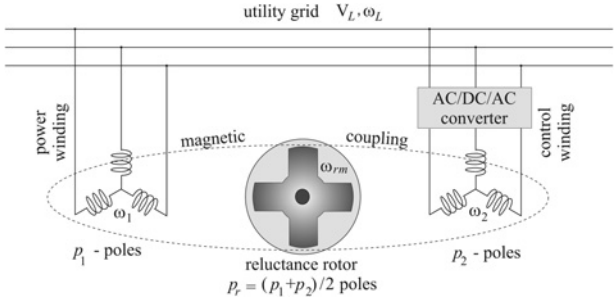

Figure 4 *Schematic connection topology of the BDFRM-WECS*

Neglecting the friction terms, the mechanical dynamic behaviour of the BDFRM-WECS can be written as

$$\dot{\omega}_{\mathrm{rm}} = \frac{1}{J}(T_{\mathrm{t}}' + T_{\mathrm{e}}) \tag{12}$$

where ω_{rm} represents the mechanical angular speed of the generator, J is the inertia of the rotating parts, T_{t}' is the torque produced by the blades of the wind turbine (referred to the generator side using the gear box constant K_{gb}) and T_{e} is the electromagnetic torque developed by the BDFRM.

The torque produced by the generator can be described by the expression ($T_{\mathrm{e}} < 0$ as generator) [8]

$$T_{\mathrm{e}} = \frac{3}{2}\frac{L_{12}}{L_1} p_{\mathrm{r}}(\lambda_{1d} i_{2q} + \lambda_{1q} i_{2d}) \tag{13}$$

where p_{r} is the number of poles in the reluctance rotor that, by construction, corresponds to half the total stator poles ($p_{\mathrm{r}} = (p_1 + p_2)/2$). At this point, it is important to stress that to produce torque this machine has to rotate at a mechanical angular speed ω_{rm} given by the expression [8]

$$p_{\mathrm{r}}\omega_{rm} = \omega_1 + \omega_2 = \omega_{\mathrm{r}} \tag{14}$$

being ω_{r} the electrical angular speed of the reluctance rotor. Then replacing (13) and (14) in (12), the mechanical dynamic behaviour of the WECS can be rewritten as

$$\dot{\omega}_{\mathrm{r}} = \frac{p_{\mathrm{r}}}{2J}\left(\frac{\rho\pi r^3}{K_{\mathrm{gb}}} C_{\mathrm{t}} v^2 + \frac{3L_{12}}{L_1} p_{\mathrm{r}}(\lambda_{1d} i_{2q} + \lambda_{1q} i_{2d})\right) \tag{15}$$

where $C_{\mathrm{t}} = C_{\mathrm{p}}/\lambda$ is the turbine torque coefficient. Therefore the WECS-BDFRM results are completely described by the fifth-order dynamic model given by (4)–(11) and (15).

3.1 Reduced order model

The dynamic model introduced in the previous subsection can be adequately simplified to obtain a reduced order model specially suitable for control design purposes. In this sense, assuming that the d-axis of the primary reference frame is aligned with the primary flux spatial vector, the primary flux dynamic equations (4) and (5) can be rewritten as

$$\dot{\lambda}_{1d} = -R_1 i_{1d} + v_{1d} \tag{16}$$

$$0 = -R_1 i_{1q} - \omega_1 \lambda_{1d} + v_{1q} \tag{17}$$

Next, considering that the voltage and frequency of the grid remain approximately constant and that the primary winding resistance is negligible ($R_1 \to 0$) [7, 20], the primary flux components can be written as $\lambda_{1d} = V_L/\omega_L$ and $\lambda_{1q} = 0$. It should be noted that this consideration implies to reduce the order model in two degrees of freedom ($\dot{\lambda}_{1d} = 0$ and $\dot{\lambda}_{1q} = 0$). Then, including the last expressions of λ_{1d} and λ_{1q} in (6), (7) and (15), and replacing the flux variables by (8)–(11), the reduced order model can be expressed in terms of the secondary currents and the electrical angular speed as

$$\dot{i}_{2d} = -\frac{L_1 R_2}{L_{eq}^2} i_{2d} - (\omega_L - \omega_{\mathrm{r}}) i_{2q} + \frac{L_1}{L_{eq}^2} v_{2d} \tag{18}$$

$$\dot{i}_{2q} = \left(\frac{L_{12} V_L}{\omega_1 L_{eq}^2} + i_{2d}\right)(\omega_L - \omega_{\mathrm{r}}) - \frac{L_1 R_2}{L_{eq}^2} i_{2q} + \frac{L_1}{L_{eq}^2} v_{2q} \tag{19}$$

$$\dot{\omega}_{\mathrm{r}} = \frac{p_{\mathrm{r}}}{2J}\left(\frac{\rho\pi r^3}{K_{\mathrm{gb}}} C_{\mathrm{t}} v^2 + \frac{3L_{12}}{L_1}\frac{V_L}{\omega_L} p_{\mathrm{r}} i_{2q}\right) \tag{20}$$

where the primary current components are related to these variables through

$$i_{1d} = \frac{V_L}{\omega_1 L_1} - \frac{L_{12}}{L1} i_{2d} \tag{21}$$

$$i_{1q} = \frac{L_{12}}{L_1} i_{2q} \tag{22}$$

In this context, the torque developed by the BDFRM and the primary reactive power injected by the system into the grid can be written as [7]

$$T_{\mathrm{e}} = -\frac{3}{2}\frac{L_{12}}{L_1}\frac{V_L}{\omega_L} p_{\mathrm{r}} i_{2q} \tag{23}$$

$$Q_1 = \frac{3}{2} V_L\left(\frac{L_{12}}{L_1} i_{2d} - \frac{V_L}{\omega_L L_1}\right) \tag{24}$$

For control purposes, it is useful to express this model under a non-linear affine structure. Thus, from (18)–(20) it is straightforward to write the reduced model as

$$\dot{\boldsymbol{x}} = \boldsymbol{F}(\boldsymbol{x}) + \boldsymbol{G}(\boldsymbol{x})\boldsymbol{u} = \begin{bmatrix} f_1(\boldsymbol{x}) \\ f_2(\boldsymbol{x}) \\ f_3(\boldsymbol{x}) \end{bmatrix} + \begin{bmatrix} g_{11} & g_{12} \\ g_{21} & g_{22} \\ g_{31} & g_{32} \end{bmatrix} \begin{bmatrix} v_{2d} \\ v_{2q} \end{bmatrix} \tag{25}$$

with $\boldsymbol{x} = [i_{2d}\ i_{2q}\ \omega_{\mathrm{r}}]^{\mathrm{T}}$, $g_{11} = g_{22} = L_1/L_{eq}^2$, $g_{12} = g_{21} = g_{31} = g_{32} = 0$, $L_{eq}^2 = L_1 L_2 - L_{12}^2$, and

$$f_1(\boldsymbol{x}) = -\frac{L_1 R_2}{L_{eq}^2} i_{2d} - (\omega_L - \omega_{\mathrm{r}}) i_{2q}$$

$$f_2(\boldsymbol{x}) = \left(\frac{L_{12} V_L}{\omega_1 L_{eq}^2} + i_{2d}\right)(\omega_L - \omega_{\mathrm{r}}) - \frac{L_1 R_2}{L_{eq}^2} i_{2q}$$

$$f_3(\boldsymbol{x}) = \frac{p_{\mathrm{r}}}{2J}\left(\rho\pi r^3 C_{\mathrm{t}} v^2 + \frac{3L_{12}}{L_1}\frac{V_L}{\omega_L} p_{\mathrm{r}} i_{2q}\right)$$

4 SOSM design

This article presents a simple multi-input controller that allows one to fulfil the control objectives introduced in Section 2 when the system is operating in a perturbed

doi: 10.1049/iet-cta.2009.0437

environment. Its design is based on high-order sliding mode (HOSM) techniques for multi-input systems. This theoretical framework has proved to be specially appropriate to cope with non-linear systems, presenting robust features with respect to system parameter uncertainties and external disturbances [13, 14]. On the other hand, HOSMs allow one to completely reduce the chattering effect (inherent to traditional sliding mode implementations) decreasing the mechanical stress on the WECS. This control feature is accomplished because the discontinuous control action is applied on higher-order time derivatives of the sliding manifold [15].

To date, there are few HOSM theoretical results for multi-input systems that hold the simplicity of the original approach for single-input single-output (SISO) systems. The main results known in this field have been obtained by Bartolini *et al.* [21] and by Levant [22]. In this article, the controller design has been faced following the approach of Levant, using an SOSM super-twisting algorithm which presents the additional advantage of needing information only of the sliding surface and not of its time derivatives. It is important to remark that the implementation of the proposed controller implies an online computational cost similar to that of a linear PI + D controller.

4.1 Design of MIMO-SOSM controllers

We consider a multi-input non-linear dynamic system model expressed under the affine structure

$$\dot{\boldsymbol{x}} = \boldsymbol{F}(\boldsymbol{x}) + \Delta\boldsymbol{F}(\boldsymbol{x}, t) + (\boldsymbol{G} + \Delta\boldsymbol{G}(t))\boldsymbol{u} + \xi(t) \tag{26}$$

where $\boldsymbol{x} \in \Re^n$ and $\boldsymbol{u} \in \Re^m$. In (26), the addition of $\boldsymbol{F}$ and $\Delta\boldsymbol{F}(\boldsymbol{x}, t)$ represents the system drift vector field. The former term corresponds to the drift vector of the nominal system whereas the latter is an explicitly time-dependent drift vector originated in slow temporal parameter variations. On the other hand, the factor composed by the addition of $\boldsymbol{G}$ and $\Delta\boldsymbol{G}(t)$ represents the system control matrix. Its first term is considered constant and corresponds to the nominal control system matrix whereas the second one, as in the previous case, takes into account the action of temporal parameter variations on the former. Finally, $\xi(t)$ is a continuous vector field representing the influence of external perturbations.

To proceed with the SOSM control design, it is necessary to define an m-order sliding manifold $\boldsymbol{S} = [s_1\ s_2 \ldots s_m]^{\mathrm{T}}$ that represents the desired control objectives and has a vectorial relative degree [1 1…1]. Then, its first time derivative can be written as

$$\dot{\boldsymbol{S}} = \underbrace{\frac{\partial \boldsymbol{S}}{\partial \boldsymbol{x}}(\boldsymbol{F}(\boldsymbol{x}) + \Delta\boldsymbol{F}(\boldsymbol{x}, t) + \xi(t))}_{L_{(F+\Delta F+\xi)}\boldsymbol{S}} + \underbrace{\frac{\partial \boldsymbol{S}}{\partial \boldsymbol{x}}(\boldsymbol{G} + \Delta\boldsymbol{G}(t))}_{L_{(G+\Delta G)}\boldsymbol{S}}\boldsymbol{u} + \frac{\partial \boldsymbol{S}}{\partial t} \tag{27}$$

Provided that $L_{(G+\Delta G)}\boldsymbol{S}$ is invertible (see vectorial relative degree condition), (27) can be manipulated according to the following variable exclusion Gauss procedure

$$\begin{cases} \widetilde{\dot{s}}_i = \dot{s}_i - \dot{s}_i \dfrac{(L_{(G+\Delta G)}\boldsymbol{S})_{i_1 j}}{(L_{(G+\Delta G)}\boldsymbol{S})_{i_1 j_1}} & \forall i \neq i_1 \text{ first step} \\ \widetilde{\dot{s}}_i = \widetilde{\dot{s}}_i - \widetilde{\dot{s}}_i \dfrac{(L_{(G+\Delta G)}\boldsymbol{S})_{i_k j}}{(L_{(G+\Delta G)}\boldsymbol{S})_{i_k j_k}} & \forall i \neq i_1, \ldots, i_{k-1}, i_k \\ & k = 2 \ldots m \end{cases} \tag{28}$$

to obtain a new expression given by

$$\widetilde{\dot{\boldsymbol{S}}} = \widetilde{L}_{(F+\Delta F+\xi)}\boldsymbol{S} + \widetilde{L}_{(G+\Delta G)}\boldsymbol{S}\boldsymbol{u} + \frac{\partial \widetilde{\boldsymbol{S}}}{\partial t} \tag{29}$$

where $\widetilde{L}_{(G+\Delta G)}\boldsymbol{S}$ presents an upper-triangular form associated with an input/output matrix assignment given by

$$\begin{pmatrix} i_1\, i_2 \cdots i_m \\ j_1 j_2 \cdots j_m \end{pmatrix} \tag{30}$$

It should be noted that this last matrix presents in its columns the position (i_k, j_k) corresponding to the successive elements of the matrix $L_{(G+\Delta G)}\boldsymbol{S}$ used as pivots during the execution of the Gauss procedure.

In case of using the super-twisting algorithm, it is proved [22] that if each control input is driven by the controller

$$\begin{aligned} u_{j_k} &= -\lambda_{j_k} |s_{i_k}|^{1/2} \operatorname{sign}(s_{i_k}) + \nu_{j_k} \quad j_k = m \cdots 1 \\ \dot{\nu}_{j_k} &= \begin{cases} -u_{j_k} & |u_{j_k}| > \widehat{U}_{j_k} \\ \alpha_{j_k} \operatorname{sign}(s_{i_k}) & |u_{j_k}| \leq \widehat{U}_{j_k} \end{cases} \end{aligned} \tag{31}$$

where the parameters α_{j_k}, λ_{j_k} and $\widehat{U}_{j_k}$ are chosen in the reverse order (taking j_k from m to 1) according to the following inequalities [22]

$$\underline{K}_{i_k} \alpha_{j_k} > C_{i_k} \tag{32}$$

$$\lambda_{j_k} > \sqrt{\frac{2}{\underline{K}_{i_k}\alpha_{i_k} - C_{i_k}}} \frac{\overline{K}_{i_k}(\underline{K}_{i_k}\alpha_{i_k} - C_{i_k})(1 - q_{i_k})}{\underline{K}_{i_k}^2 (1 - q_{i_k})} \tag{33}$$

$$0 < q_{i_k} < 1 \tag{34}$$

$$0 < \underline{K}_{i_k} < (L_{(G+\Delta G)}\boldsymbol{S})_{i_k j_k} < \overline{K}_{i_k} \tag{35}$$

$$\left| \left(\widetilde{\dot{L}}_{(F+\Delta F+\xi)}\boldsymbol{S} + \frac{\partial^2 \widetilde{\boldsymbol{S}}}{\partial t^2} \right)_{i_k} \right| + \sum_{j_k} |(\widetilde{\dot{L}}_{(G+\Delta G)}\boldsymbol{S})_{i_k j_k}| \widehat{U}_{j_k} \leq C_{i_k} \tag{36}$$

$$\left| \left(\widetilde{L}_{(F+\Delta F+\xi)}\boldsymbol{S} + \frac{\partial \widetilde{\boldsymbol{S}}}{\partial t} \right)_{i_k} / (\widetilde{L}_{(G+\Delta G)}\boldsymbol{S})_{i_k j_k} \right| < q_{i_k} \widehat{U}_{j_k} \tag{37}$$

the system reaches the sliding manifold $\boldsymbol{S}$ in finite time and stays on it without chattering. It should be noted that all these inequalities are simple extensions of the ones corresponding to the SISO case [15, 23].

It is important to remark that the controller (31) ensures the convergence to the manifold $\boldsymbol{S} = 0$ for any operational environment that preserves (34)–(37). This means that if the second time derivatives of the sliding variables belong to the differential inclusions

$$\ddot{s}_{i_k} \in [-C_{i_k}\ C_{i_k}] + [\underline{K}_{j_k}\ \overline{K}_{j_k}]\dot{u}_j \quad k = 1 \cdots m \tag{38}$$

the dynamic system converges towards the manifold $\boldsymbol{S} = 0$. As the inclusions involved in (38) do not remember the original dynamic system, the super-twisting controller is robust against any perturbation that preserves them.

4.2 Application to the WECS-BDFRM system

As it was previously mentioned, the control objective is to maximise the total active power delivered by the system and to simultaneously regulate the reactive power injected by the primary winding into the grid. For the sake of simplicity on the control design phase, the controller is developed using the reduced dynamic order model obtained in Section 3.1. Then, taking into account the power references previously obtained in Section 2, the control objectives can be expressed in terms of the following two sliding variables

$$s_1(\boldsymbol{x}) = \frac{K_{\text{opt}}}{p_{\text{r}}^2 K_{\text{gb}}^2}\omega_{\text{r}}^2 + \frac{3}{2}\frac{L_{12}}{L_1}\frac{V_L}{\omega_L}p_{\text{r}} i_{2q} \tag{39}$$

$$s_2(\boldsymbol{x}) = Q_{1\text{ref}}(t) - \frac{3}{2}V_L\left(\frac{L_{12}}{L_1}i_{2d} - \frac{V_L}{\omega_L L_1}\right) \tag{40}$$

At this point, it should be remembered that although (39) is expressed in terms of torque values referred to the generator side, this sliding variable allows to follow a filtered version of the maximum conversion point and therefore to maximise the active power conversion [19]. Besides, using a sliding variable in terms of torque simplifies the controller tuning procedure because the expression corresponding to the machine torque involves only one state variable. On the other hand, it is important to note that the sliding vector $\boldsymbol{S} = [s_1\ s_2]^{\text{T}}$ presents the required vectorial relative degree to carry out the MIMO-SOSM design method outlined in the previous subsection. Then, including on the dynamic model (25) all the uncertainties and perturbations considered in the previous subsection, the time derivative of $\boldsymbol{S}$ can be written as

$$\dot{\boldsymbol{S}} = \underbrace{\begin{bmatrix} \dfrac{3L_{12}V_L}{2L_1\omega_L}(p_{\text{r}}(f_2 + \Delta f_2(t) + \xi_2(t)) \\ \quad + \dfrac{2K_{\text{opt}}\omega_{\text{r}}}{p_{\text{r}}^2 K_{\text{gb}}^2}(f_3 + \Delta f_3(t) + \xi_3(t))) \\ -\dfrac{3L_{12}V_L}{2L_1}(f_1 + \Delta f_1(t) + \xi_1(t)) + \dfrac{\partial Q_{1\text{ref}}}{\partial t} \end{bmatrix}}_{L_{(F+\Delta F+\xi)}\boldsymbol{S}+\frac{\partial \boldsymbol{S}}{\partial t}}$$
$$\underbrace{-\frac{3L_{12}V_L}{2L_1}\begin{bmatrix} 0 & -\dfrac{p_{\text{r}}}{\omega_L}\left(\dfrac{L_1}{L_{eq}^2} + \Delta g_{22}(t)\right) \\ \left(\dfrac{L_1}{L_{eq}^2} + \Delta g_{11}(t)\right) & 0 \end{bmatrix}}_{L_{(G+\Delta G)}\boldsymbol{S}} \boldsymbol{u} \tag{41}$$

$L_{(G+\Delta G)}\boldsymbol{S}$ being anti-diagonal it is not necessary to follow the Gauss exclusion procedure. Each sliding variable is related to only one control variable, determining a fixed output/input matrix assignment.

In order to choose the controller parameters α_i, λ_i and $\widehat{U}_i$ for $i = 1, 2$, it is necessary to obtain the analytic expressions corresponding to the second time derivative of the sliding surfaces. Next, after long but straightforward algebraic manipulations bounds (34)–(37) are obtained regarding the operational limits and the maximum levels of perturbations and unmodelled dynamics acting on the system. After this analytic procedure, the controller parameters are selected according to (32) and (33) to obtain a good reaching performance. This last tuning phase can be realised analytically or using simulation tools. In this case, the controller parameter values chosen for the VSCF-BDFRM generation system were obtained following the latter procedure and are specified in the Appendix. For the sake of clarity, it is important to remark that the bounding constants and the controller parameters are computed offline only once during the controller tuning procedure.

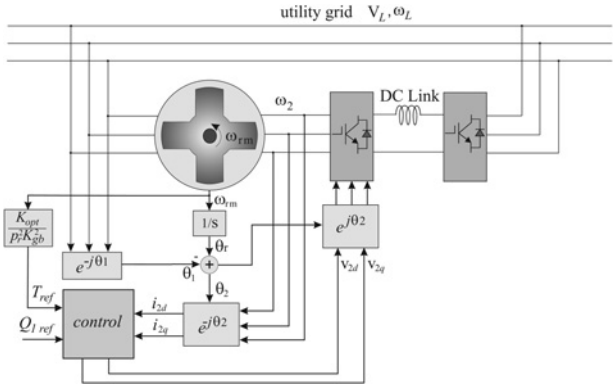

Figure 5 *Schematic closed-loop system*

doi: 10.1049/iet-cta.2009.0437

Therefore computational online operation of the control algorithm (31) is very simple.

Finally, a schematic block diagram showing the closed-loop system topology is presented in Fig. 5. It should be noted that the controller implementation only requires the measurement of the secondary current components, the rotational speed (also necessary to calculate the *dq* transformations) and the utility grid voltages.

5 Simulation results

To demonstrate the chattering-free controller behaviour, its good robustness properties against unknown disturbances and unmodelled dynamics and its very good tracking performance, computer-aided simulations were performed and are presented in this section. Furthermore, simulations using a traditional linear control scheme based on proportional-integral-derivative (PID) controllers (having a similar computational cost to the SOSM approach) are presented in this section in order to establish a basis for performance comparisons.

To recreate the system operation under realistic conditions, simulations were carried out with the controller synthesised in Section 4.2 driving the BDFRM-WECS represented by its complete dynamic model. It should be noted that this controller was designed considering the reduced order system model. External variables, references and disturbances were included through representative time profiles which are separately depicted in Figs. 6 and 7. In particular, Fig. 6 shows the wind speed time profile (v) and the primary reactive power reference ($Q_{1\text{ref}}$). The former includes wind speed variations within the partial-load operation zone, that is, wind speeds below the value where the generator develops its rated power. On the other hand, the latter presents a stepped feature that represents sudden changes imposed by a high-level grid operation controller according to reactive line compensation necessities.

External disturbances and model uncertainties owing to parameter variations are considered on the dynamic model through the terms ξ and $\Delta\boldsymbol{F} - \Delta\boldsymbol{G}$, respectively (see (26)). Fig. 7 shows the time profiles corresponding to the external disturbances used in the simulations. These variations are presented using a percentage scale that takes the maximum value of the corresponding drift field vector element ($f_{i\,\max}$) as reference. On the other hand, model uncertainties were included considering the parameter variations depicted in

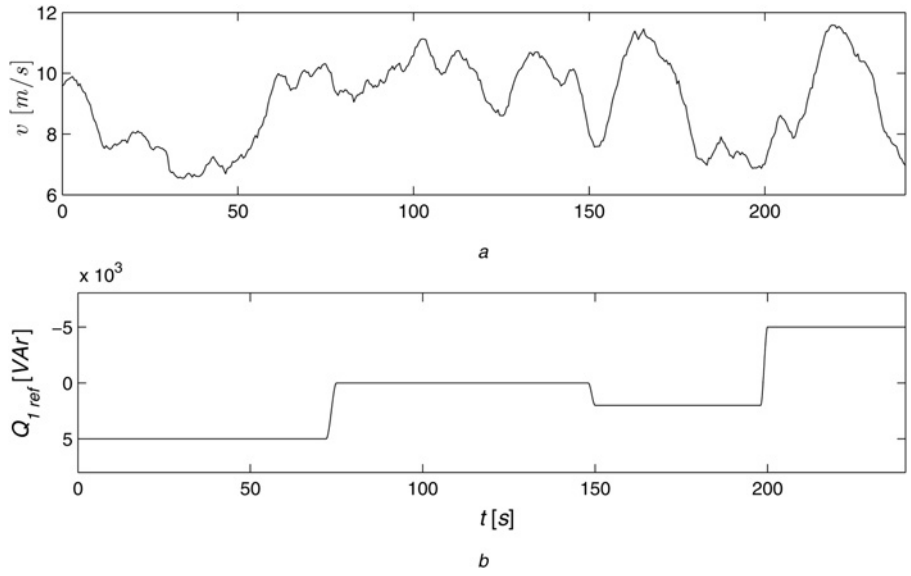

Figure 6 *External variables*

a Wind speed *v*
b Primary reactive power reference $Q_{1\text{ref}}$

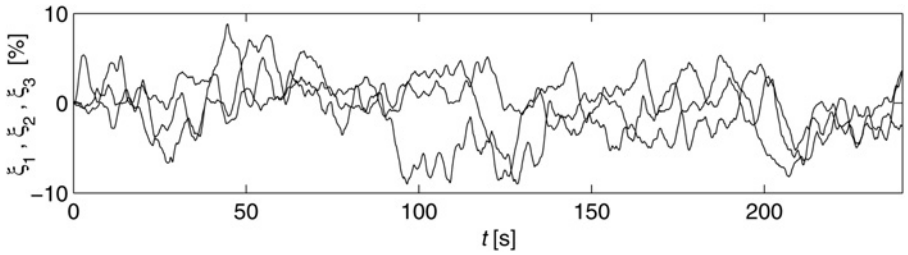

Figure 7 *Disturbance components ξ_1, ξ_2 and ξ_3*

Fig. 8. It should be noted that these variations are also shown in a percentage scale that takes the respective nominal values as references. Remember that $L_1 = L_{lp} + L_m$, $L_2 = L_{ls} + L_m$ and $L_{12} = L_m$, where L_{lp} and L_{ls} are the leakage inductances of the primary and secondary winding, respectively, and L_m is the magnetising inductance.

The closed-loop system performance can be analysed through the behaviour of the sliding variables s_1 and s_2. Their profiles, presented in Fig. 9, prove that the designed controller is capable of strictly maintaining the condition $s_i = \dot{s}_i = 0$, $i = 1, 2$, without chattering even in the perturbed environment recreated for these simulations. For comparison purposes, this figure also includes the simulations corresponding to a PI-based control scheme that has given the best results. This last control scheme is composed by two independent PI controllers whose parameters have been selected by linearising the system (around the mean wind speed and a primary reactive power equal to zero) and tuning the controllers using simulation tools to obtain the fastest tracking speed without overshot. The decision of using two independent PI controllers instead of a MIMO-PI version is justified by the Bristol's interaction index obtained for the previous linearised system ($\lambda_{BI} = 1.015$) [24, 25]. This index (a simplification of the Bristol's relative gain array for two-input two-output systems) is a simple measure of interaction between the control loops for low-frequency signals. A Bristol's index equal to 1 implies no interaction between loops whereas small or negative values indicate that there are interactions.

As it can be seen in Fig. 9, the SOSM controller shows better robustness properties in an extended operation range than its PI counterpart, having a similar computational load. On the other hand, Fig. 10 shows the profile of the maximum power available in the wind, P_w (in solid line), and the electromagnetic power converted by the BDFRM, P_g (in dashed line). It can be observed in this figure that

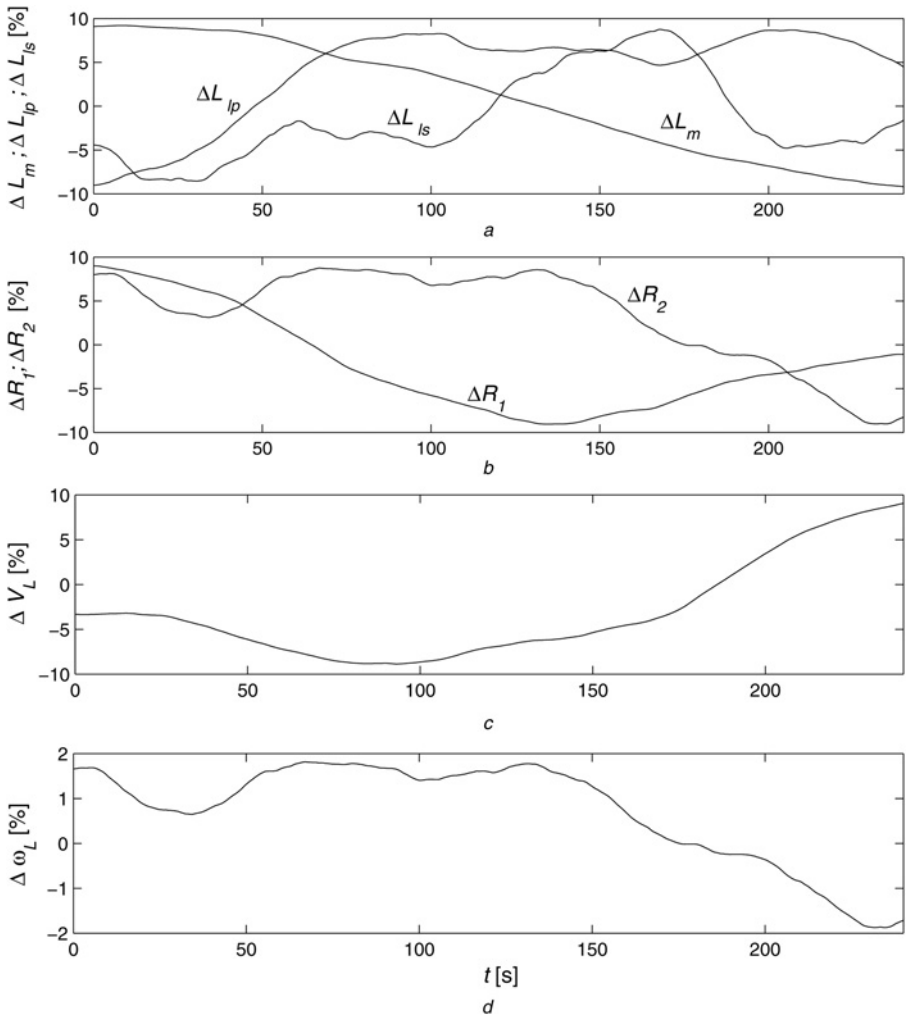

Figure 8 *Parameter variations*

a BDFRM winding inductance variations
b BDFRM winding resistance variations
c Grid voltage variation
d Grid frequency variation

doi: 10.1049/iet-cta.2009.0437

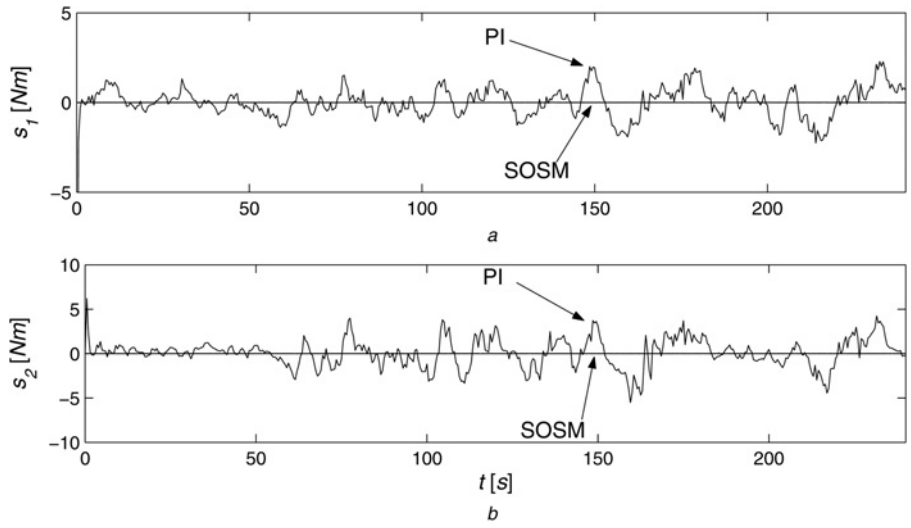

Figure 9 *Sliding variables in*
a Torque sliding surface, s_1
b Primary reactive surface, s_2

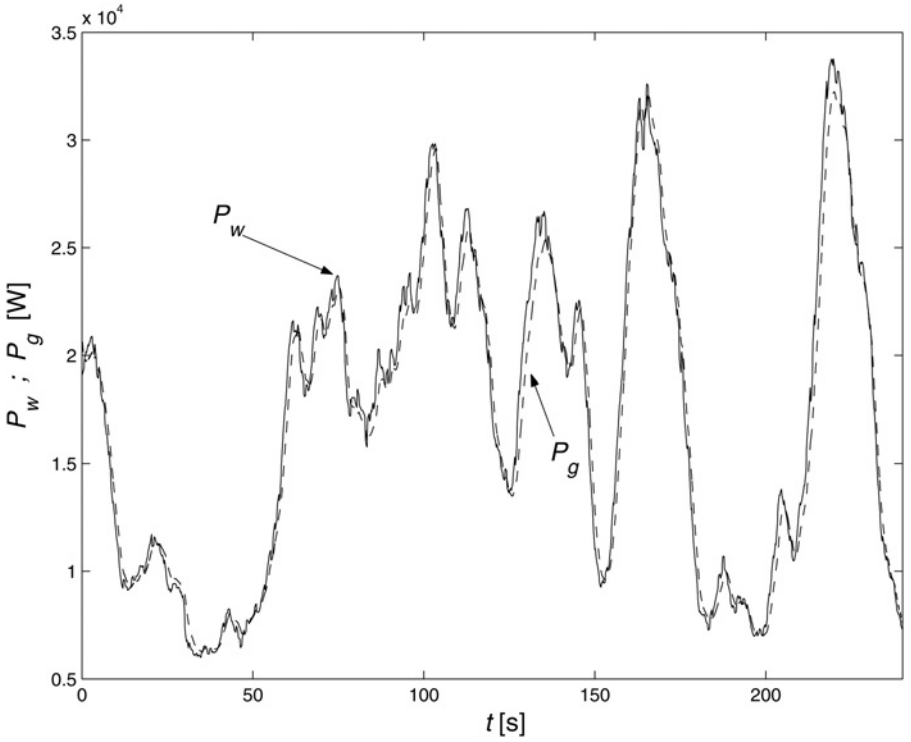

Figure 10 *Active power generation*

the controlled system is capable of closely following the maximum power conversion point even when the proposed controller is not measuring the wind speed. It is also important to note that on periods where the wind speed falls, the converted power is greater than the available power in the wind. This is possible because during those periods the system reduces its shaft speed in order to follow the maximum power conversion point and therefore the kinetic energy associated with this deceleration is converted to electromagnetic power.

To complete the analysis, Figs. 11 and 12 present the time profiles of the system states and the control variables. In particular, Fig. 11*a* shows the primary winding currents: i_{1d} and i_{1q}. The stepped feature appreciated in the former is inherently related to the time variation of the reactive power reference. Fig. 11*b* depicts the secondary winding currents: i_{2d} and i_{2q}. It should be observed that these last profiles are closely related to the primary ones (see approximations (21) and (22)). Finally, Fig. 11*c* presents the time profile of ω_{rm}.

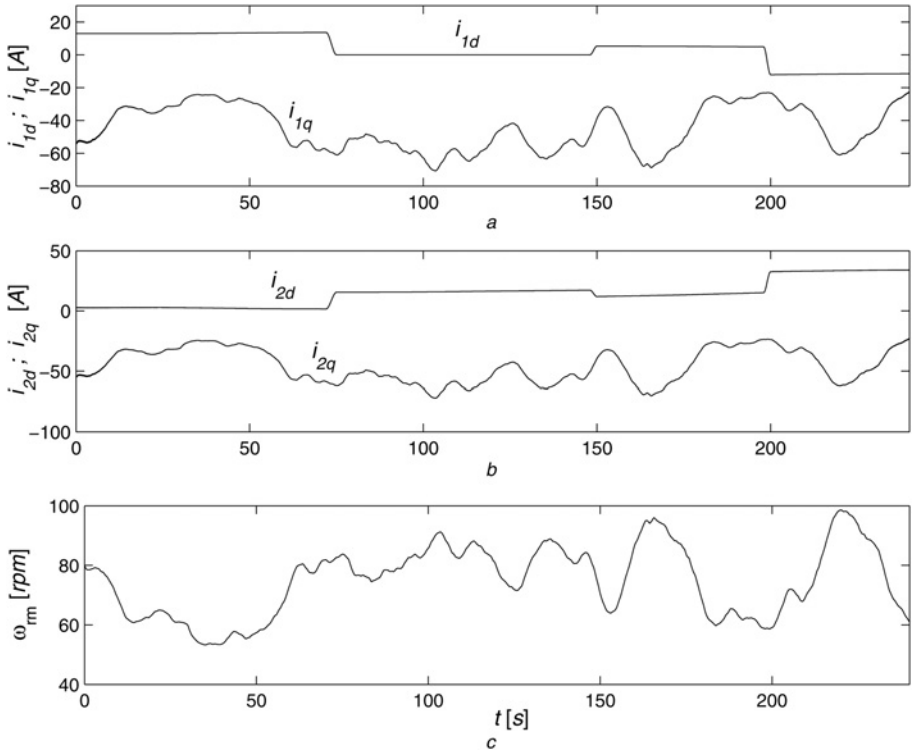

Figure 11 *System variables*

a i_{1d} and i_{1q}
b i_{2d} and i_{2q}
c ω_{rm}

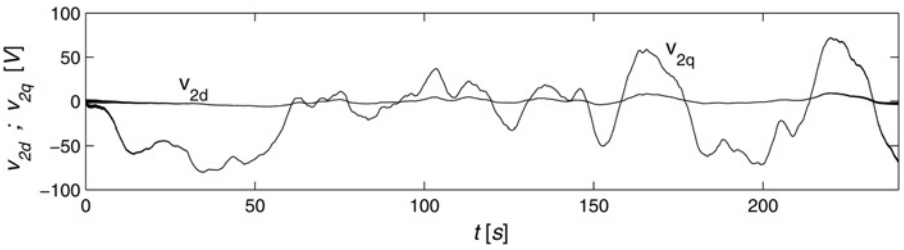

Figure 12 *Control voltages: v_{2d} and v_{2q}*

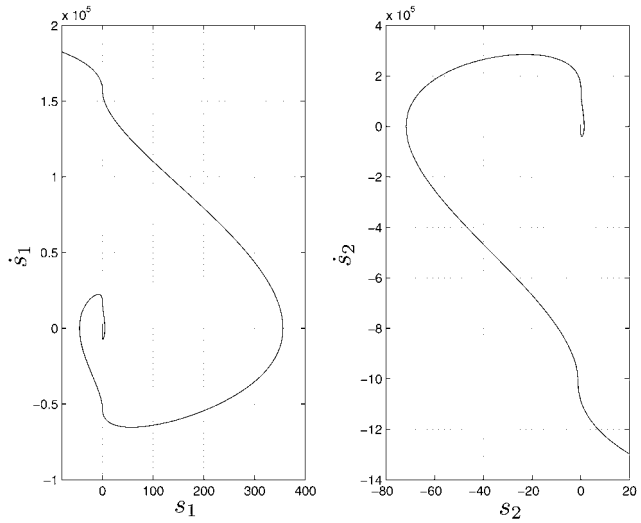

Figure 13 *Reaching phase portrait of s_1 and s_2*

On the other hand, Fig. 12 shows the control variables v_{2d} and v_{2q}. It is important to stress their smoothness features determined by the use of SOSM control techniques. This chattering-free characteristic is specially attractive because it reduces the mechanical stress on the system and because these voltages can be synthesised by the bidirectional static converter placed at the secondary winding terminals.

Finally, in Fig. 13, the phase portraits corresponding to the system reaching phase are separately depicted. These plots show the typical form that systems controlled by super-twisting algorithms draw during convergence.

6 Conclusions

This paper presents the design of a MIMO-SOSM controller that allows one to simultaneously maximise the

doi: 10.1049/iet-cta.2009.0437

active power generation of a BDFRM-WECS and to regulate the reactive power injected by the generator into the utility grid. In this way, the developed control allows one to use the system not only as an active power generator but also as a partial reactive line compensator.

The control was designed using an SOSM super-twisting algorithm for multi-input systems, which is very appropriate to deal with non-linear system models operating in perturbed environments. The controlled closed-loop system shows very good performance with additional attractive features like a chattering-free behaviour, a finite reaching time phase, and excellent robustness properties against external disturbances and unmodelled dynamics. These control features were corroborated through representative simulations. Finally, it should be stressed that the implementation of the proposed controller does not require more computational cost than necessary to implement a control scheme based on traditional PIDs.

7 Acknowledgments

This work was supported by the National University of La Plata (UNLP), the Consejo Nacional de Investigaciones Científicas y Técnicas (CONICET) and the SECyT.

8 References

[1] 'Global wind energy outlook'. Global Wind Energy Council Report, 2006, http://www.gwec.net/

[2] BIANCHI F., DEBATTISTA H., MANTZ R.: 'Optimal gain-scheduled control of fixed-speed active stall wind turbines', *IET Renew. Power Gener.*, 2007, **2**, (4), pp. 228–238

[3] SODER L., HOFMANN L., ORTHS A., HOLTTINEN H., WAN Y., TUOHY A.: 'Experience from wind integration in some high penetration areas', *IEEE Trans. Energy Convers.*, 2007, **22**, (1), pp. 4–12

[4] BELTRAN B., AHMED-ALI T., BENBOUZID M.: 'Sliding mode power control of variable-speed wind energy conversion systems', *IEEE Trans. Energy Convers.*, 2008, **23**, (2), pp. 551–558

[5] JOVANOVIC M., AHAMED M.: 'Sensorless speed control strategy for brushless doubly-fed reluctance machines'. Electric Machines and Drives Conf., IEMDC'07, 2007, pp. 1514–1519

[6] TANG Y., XU L.: 'A flexible actice and reactive power control for a variable speed constant frequency generating system', *IEEE Trans. A Control*, 1995, **10**, (4), pp. 472–478

[7] XU L., ZHEN L., KIM E.: 'Field orientation control of a doubly excited brushles reluctance machine', *IEEE Trans. Ind. Appl.*, 1998, **34**, (1), pp. 148–155

[8] JOVANOVIC M., BETZ R., YU J.: 'The use of doubly fed reluctance machines for large pumps and wind turbines', *IEEE Trans. Ind. Appl.*, 2002, **38**, (6), pp. 1508–1516

[9] JOVANOVIC M., YU J., LEVI E.: 'Encoderless direct torque controller for limited speed range aplications of brushless doubly fed reluctance motors', *IEEE Trans. Ind. Appl.*, 2006, **42**, (3), pp. 712–722

[10] JOVANOVIC M., BETZ R.: 'Slip power recovery systems based on brushless doubly fed reluctance machines'. Power Control Conf., PCC'02, 2002, pp. 987–992

[11] JOVANOVIC M., BETZ R., YU J., LEVI E.: 'Aspects of vector and scalar control of brushless doubly fed reluctance machines'. Power Electronics and Drive Systems, PEDS'01, 2001, pp. 461–467

[12] JOVANOVIC M., YU J., LEVI E.: 'A doubly fed reluctance motor drive with sensorless direct torque control'. Electric Machines and Drives Conf., IEMDC'03, 2003, pp. 1518–1524

[13] LEVANT A.: 'Sliding order and sliding accuracy in sliding mode control', *Int. J. Control*, 1993, **58**, (6), pp. 1247–1263

[14] BARTOLINI G., PISANO A., PUNTA E., USAI E.: 'A survey of applications of second order sliding mode control to mechanical systems', *Int. J. Control*, 2003, **76**, (9/10), pp. 875–892

[15] FRIDMAN L., LEVANT A.: 'Higher order sliding modes', PERRUQUETTI W., BARBOT J.P. (EDS): 'Sliding mode control in engineering' (Marcel Dekker, Inc., 2002), Ch. 3, pp. 53–101

[16] LEVANT A.: 'Introduction to high-order sliding modes', 2003, http://www.tau.ac.il/levant/hosm2002.pdf

[17] TAPIA A., TAPIA G., OSTOLAZA J.: 'Reactive power control of wind-farms for voltage control applications', *Renew. Energy*, 2004, **29**, pp. 377–392

[18] FRERIS L.L.: 'Wind energy conversion systems' (Prentice Hall, 1990)

[19] EKANAYAKE J., HOLDSWORTH L., WU X., JENKINS N.: 'Dynamic modeling of doubly fed induction generator wind turbines', *IEEE Trans. Plasma Sci.*, 2003, **18**, (2), pp. 803–809

[20] XU L., TANG Y.: 'A novel wind-power generating system using field orientation controlled doubly-excited brushles reluctance machine'. IEEE Industry Applications Society Ann. Meeting, 1992, pp. 408–413

[21] BARTOLINI G., FERRARA A., USAI E., UTKIN V.: 'On multi-input chattering-free second-order sliding mode control', *IEEE Trans. A Control*, 2000, **45**, (9), pp. 1711–1717

[22] LEVANT A.: 'MIMO 2-sliding control design'. European Control Conf., Cambridge, UK, 2003

[23] BARTOLINI G., PISANO A., PUNTA E., USAI E.: 'On second order sliding mode controllers', SABANOVIC A., FRIDMAN L., SPURGEON S. (EDS): 'Variable structure systems: from principles to implementation' (Springer-Verlag, 2004), Ch. 17, pp. 329–350

[24] ASTRÖM K.J., HÄNGGLUND T.: 'Advanced PID control' (Taylorand Francis, 2006)

[25] SKOGESTAD S., POSTLETHWAITE I.: 'Multivariable feedback control. Analysis and design' (John Willey and Sons, 1998)

9 Appendix

Utility grid parameters

$$V_L = 460\,\mathrm{V} \quad \omega_1 = 2\pi 50\,\mathrm{rad/s}$$

Turbine parameters

$$r = 5.3\,\mathrm{m} \quad \rho = 1.22422\,\mathrm{kg/m^3} \quad \lambda_{\mathrm{opt}} = 5.5$$

$$C_{\mathrm{popt}} = 0.4 \quad K_{\mathrm{gb}} = 8 \quad J = 6.82\,\mathrm{kg\,m^2}$$

BDFRM parameters

$$P = 37\,\mathrm{kW} \quad p_{\mathrm{r}} = 4 \quad R_1 = R_2 = 0.012\,\Omega$$

$$L_1 = L_2 = 0.0473\,\mathrm{H} \quad L_{12} = 0.0465\,\mathrm{H}$$

SOSM controller parameters

$$\alpha_1 = 5000 \quad \lambda_1 = 1.2 \quad \widehat{U}_1 = 500$$

$$\alpha_2 = 8000 \quad \lambda_2 = 0.275 \quad \widehat{U}_2 = 100$$

PI controller parameters

$$T_{i1} = 0.009 \quad K_{p1} = 0.072$$

$$T_{i2} = 0.11 \quad K_{p2} = 0.044$$

doi: 10.1049/iet-cta.2009.0437